Vilnius University

Faculty of Physics

Institute of applied electrodynamics and telecommunications

Shamika Mahadevaiah

Dielectric spectroscopy of High Entropy Perovskite Ceramics

Master's final thesis

Electronics and telecommunication programme

Student	Shamika Mahadevaiah
Approval	2026-05-22
Academic supervisor	Dr. Jūras Banys
Director of the Institute of Applied Electrodynamics and Telecommunications	prof. Robertas Grigalaitis

Vilnius 2026

Table of Contents

Introduction

With the global energy consumption on a rise, it is high time to combine the energy harvesting technologies with energy storage devices. For this purpose, lead-free ceramic capacitors come into the role in energy storage devices due to their super ability that is fast charging and discharging. High-entropy ceramics, which are defined as the solid containing more than or equal to five components in an equiatomic system have been gaining attention due to their remarkable properties and the huge application potential in the field of energy storage.[1][2]
This work aims to investigate the dielectric properties of the high-entropy ceramic solid $(Ba_{0.2}Sr_{0.2}Ca_{0.2}La_{0.2}X_{0.2})TiO_3$ (BSCLX) where X=Li, K, Ag, Cs and Na. To meet current demands for high-entropy ceramics, a La-modified BSCLX system (BSCLX-L) is developed. Lanthanum is incorporated to stabilize a single-phase structure at high temperatures while maintaining good dielectric properties and enabling stable performance over a broad frequency range. Here the measurement of dielectric properties such as real part (energy storage) and imaginary part (energy loss) of the samples is done and their behaviour to the temperature changes according to the frequencies is observed.

1. Literature overview

1.1 Dielectric material

Dielectric materials which are excellent in their dielectric properties are employed as insulators. An important property of a dielectric is its ability to support an electrostatic field while dissipating minimal energy in the form of heat. A dielectric material is more effective the lower the proportion of energy lost as heat (dielectric loss). The other is the dielectric constant which is the concentration of the electrostatic lines of flux occurring in a substance. A low value of dielectric constant is exhibited by a perfect vacuum, dry air, and most pure dry gases like helium and nitrogen. Material of intermediate dielectric constants are ceramics, distilled water, paper, mica, polyethylene and glass. An example of a dielectric is placing a ceramic material between the metallic plates of a capacitor. Once the voltage across the dielectric material exceeds a critical value or the electrostatic field strength exceeds a critical value the material will suddenly conduct current.[3]

1.2 Perovskite structure

The crystal structure of perovskites is represented by the ABX_3 formula and demonstrates a huge variety of chemical compositions and structural variations. The crystal structure and symmetry of perovskite is a three-dimensional network of corner-sharing BX_6 octahedra, where ‘B’ cations occupy the octahedral centres and ‘X’ anions reside at the corners . The ‘A’ cations are situated in the larger cubic sites between the octahedra. This results in the general formula ABX_3, where ‘A’ is typically a larger cation (e.g., La, Ba) occupying the A-site, ‘B’ is a smaller transition metal cation (e.g., Ti, Mn) at the B-site, and ‘X’ is an anion (e.g., O, F) bonding to both ‘A’ and ‘B’. Many materials are stable in the ambient conditions in the cubic perovskite structure but would be distorted in other temperatures and pressures or be able to undergo a phase transition when subjected to other chemical substitutions. [4]

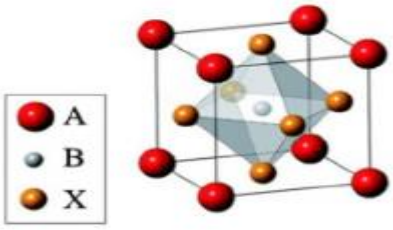

Figure1. Perovskite Structure [4].

A-site and B-site cation substitutions: Perovskite can be substituted with both A and B cations, resulting in a huge range of materials with specific properties. The lattice parameters, stability, and sometimes the introduction of charge carriers by substitution of A-site cations can be affected. For example, by replacing La with Ca in the compound $LaMnO_3$ the electronic properties of the compound can be changed. Likewise, the magnetic interactions and electronic configurations in the octahedral framework can change due to B-site cation substitutions . The flexibility enables researchers to fine-tune properties like magnetism and conductivity. [4]

1.3 High Entropy Ceramics

The HEA was first introduced in 2004. Later in the year 2015 High Entropy concept was extended to the field of Ceramics, and the five-component oxide rock salt was reported. The figure depicts the enhancement of entropy with the number of components that stabilize the system and form a single-phase solid solution. Similar to HEAs solid solutions of inorganic compounds (five or more cations sublattices) with one or more sites shared by equal atomic ratios of multi-principal elements are known as High Entropy ceramic (HEC) . High Entropy Ceramics (HEC) can be defined (a) as having at least five elements with a percentage between 5 - 35% or (b) having an entropy greater than 1.5R .An ideal HEC should be a single-phase solid solution, having a lattice with long-range periodicity but compositional disorder, i.e. the periodic lattice sites contain the constitute atoms in a random way .[5]

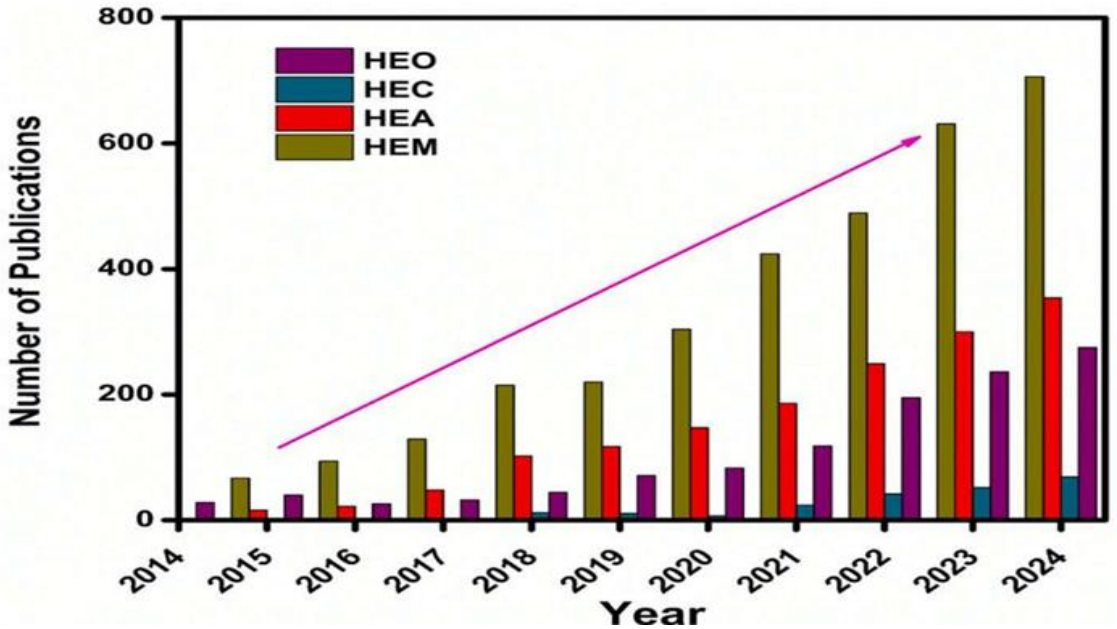

Fig 2. Chart showing the number of publications during the last 10 years using the keywords High Entropy Oxide (HEO), High Entropy ceramics (HEC), High entropy Alloy (HEA) and High entropy material (HEM). [5].

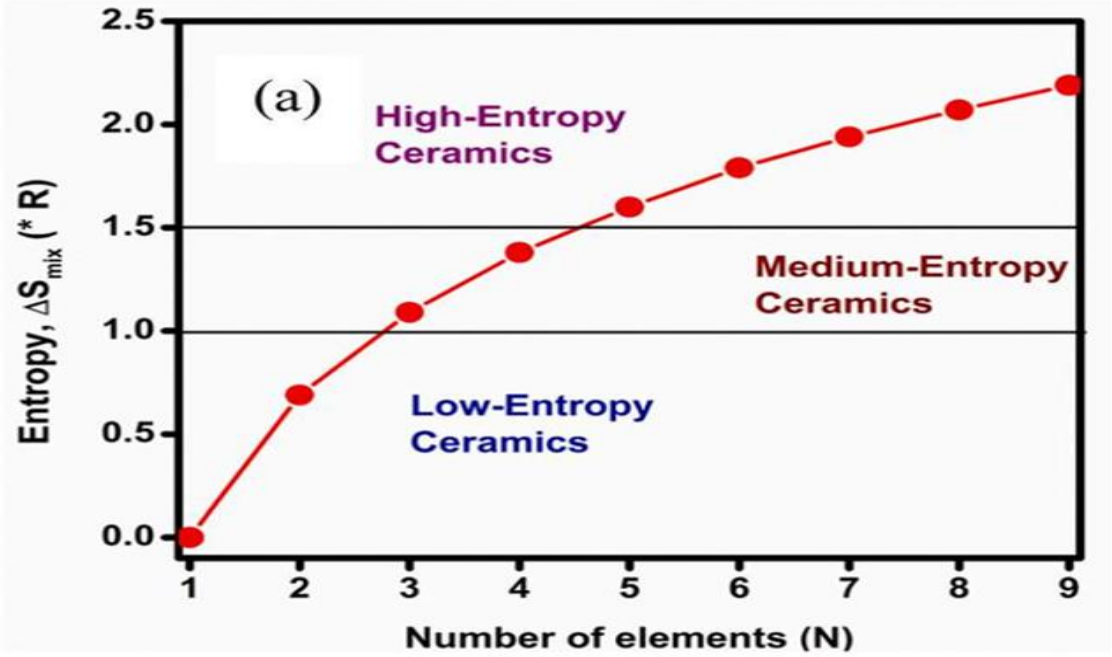

Fig 3. ΔS_{mix} as a Function of number of constituent elements. [5]

For ideal solid solution the ideal configurational entropy (mixing entropy) of mixing per mole is given by the following equation

$S_{mix} = -R\sum_{i-1}^{N} x_i ln x_i$ where R is the gas constant, x_i is the molar fraction of the ith element, and N is the total number of the constituent elements. Normally, alloys with ΔS_{mix} >1.61 R are

classified as HEAs, alloys with $0.69R < \Delta S_{mix} < 1.61$ R are called medium-entropy alloys, and alloys with $\Delta S_{mix} < 0.69$ R are called low-entropy alloys. The complex structure and disorder of the materials have a significant impact on the electrical behaviour of material. [5]. The main goal of this thesis is to measure the dielectric properties of the HEC material and to see which material has good storage property with less loss.

The structural stability of perovskite structure is generally expressed by the Goldschmidt tolerance factor (t) which is defined as

$$t = \frac{\mathrm{Ra} + \mathrm{Ro}}{\sqrt{2}\,(\mathrm{Rb} + \mathrm{Ro})} \tag{1}$$

Where R_a R_o R_b effective ionic radii of A-site B-site cations and oxygen in perovskite oxides. [5]

1.4 Principles and design of HEOC

In an ideal situation, the configuration entropy in high entropy materials can be calculated

$$S_{config} = -R\,\Sigma\, x_i\, ln x_i \tag{2}$$

S_{config} is the molar configuration entropy of the mixture, R is the molar gas constant [8.314 J/(mol·K)], and x_i represented the number of moles of the i-th component. So, Sarkar et al. derived a single equation from previous studies that allows them to calculate the configurational entropy of high entropy oxides with two cation sites ($A_xB_yO_z$), A and B, as illustrated in equation.

$$S_{config} = -R\,[x\left(\sum_{i=1}^{M} x_i \ln x_i\right) i - site + y\,(\sum_{j=1}^{N} y_i \ln y_i) j - site + (\sum_{0=1}^{P} z_o \ln z_o)\, o - site \tag{3}$$

Where the particle numbers for each of the three sites are M, N, and P and x_i, y_j, and z_o are the molar fractions of the particles at A, B, and O^{2-} site respectively. The contribution of O^{2-} sites to configuration entropy is quite minimal nearly insignificant. In crystal structures with only a single type of cation site (such as rock salt type, fluorite type), by modifying the equations above we get

$$S_{config} = -R[x(\sum_{i=1}^{M} x_i \ln x_i) \quad (4)$$

In particular if all of the components are fully mixed and there is no interaction between them. The energy of HEOCs is simply the sum of their individual energies. [6]

1.5 Effects in High entropy Ceramics (HEC)

Lattice distortion effect in structure: Disorder in (HEOC) (High entropy oxide ceramics) structure in the crystal lattice the atoms have different sizes, different bonding . In means that it is impossible to have a perfect crystal structure. This results in the lattice to bend and uneven in different spots. They get locally distorted this happens due to atoms of different kind mixed.

The sluggish effect :Atoms in these materials primarily move via utilizing vacancies, which are empty spaces in the lattice, due to lattice distortion. However, the distortion makes it more difficult for atoms to locate and utilize these vacancies, slowing their motion . The term "sluggish diffusion effect" refers to this slowing down of atomic motion.

The cocktail effect: Mixing of different elements, different interactions of elements when they are mixed. This interaction forms a new enhanced property which is not predicted by the individual elements .[6]

1.6 Preparation process of HEOCs

The preparation process of high entropy ceramics can be summarized as follows in different synthesis environments: to obtain high entropy ceramics there are three main preparation methods. Two crystal structure diagrams of pyrochlore type HEOCs. G. Du et al. Journal of Material Research and Technology classify into three categories: Solid-phase method, liquid-phase method and gas phase.

Solid phase method

High entropy materials have been synthesised using the solid-state diffusion process at high temperature solid state diffusion is used to produce chemically stable phases. It has a wide application in the preparation of bulk materials and powder materials.[6]

Liquid phase method

High-purity, high-quality, high-entropy, oxide powder particles can be made using the liquid phase approach at low temperatures because metal cations are well dispersible in the liquid phase. There were numerous preparation steps involved in the liquid phase approach, including

Sol gel (SG) , Solution combustion (SC) , Spray pyrolysis (SP) , Electrospinning (ES) etc.[6] The sol-gel technique has proved to be a highly effective synthesis technique to obtain perovskite oxides of controlled composition and structure. Sol-gel process has many merits compared to the traditional solid-state processes and especially useful for the preparation of complex oxide system. [7]

Table 1 :Advantages and disadvantages of typical solid-phase, liquid-phase [6]

Type	Method	Shape	Advantages	Disadvantages
Solid- phase	CS	Massive、Disc- shaped	Simple equipment, low cost	Time-consuming, high-energy consumption
Solid- phase	SPS	Massive、Disc- shaped	Fast heating, short sintering time, high sintering activity, high densification	high equipment requirements
Solid- phase	RFS	Massive、Disc- shaped	Fast sintering rate, relatively simple equipment	Difficulty in obtaining uniform microstructure, low utilization of raw materials
Solid- phase	UHS	Massive、Disc- shaped	Uniform temperature distribution, short sintering cycle	Reaction speed is too fast, difficult to control organizational properties
Solid- phase	MWS	Massive、Disc- shaped	No heat source required, low-temperature rapid sintering,	Uneven heating, not at a mature industrialized level

			energy efficient, high production efficiency	
Liquid- phase	SG	Powder	Synthesizable and homogeneous at lower temperatures	Long reaction time
Liquid- phase	SC	Powder	Costs are controllable, high product purity, fast reaction speed	Difficult to control the combustion process and product shape
Liquid- phase	SGSC	Powder	Uniform composition of the product, controllable morphology, good crystal structure	Requires selection of complexing agents and metal ions, limitations on specific reactants[6]

Table 2:Summary of the sol–gel method for perovskite oxide synthesis: process steps, advantages, and disadvantages [7]

Step	Description/purpose	Advantages	Disadvantages
Precursor Selection	Choosing suitable metal alkoxides or nitrates for A- and B-site cations	High purity and stoichiometry control	Precursors can be expensive or sensitive to moisture
Chelation and Sol Formation	Stabilizing metal ions using chelating agents (e.g., citric acid, EDTA)	Prevents premature precipitation; enables molecular-level mixing	Requires careful control of pH and reagent ratios

Hydrolysis and Condensation	Forming a stable sol through hydrolysis and polycondensation reactions	Produces uniform and homogeneous distribution of elements	Reaction kinetics are sensitive to humidity, temperature, and pH
Gelation	Conversion of sol into a 3D gel network	Good compositional control; encapsulates metal ions uniformly	Gel drying can induce cracking or shrinkage
Drying	Removing solvents to form xerogel	Reduces volume and prepares material for crystallization	Risk of pore collapse or uneven drying
Calcination	Thermal treatment to decompose organics and form crystalline perovskite structure	Lower temperatures than solid-state methods; fine particle control	Can cause agglomeration or loss of volatile components if not optimized[7]

1.7 Maxwell-Wagner-Sillars interfacial polarization and Interfacial/space charge polarization

The electrical point of view of an interface is an internal surface between two phases where the electrical and dielectric properties are different. If there are internal surfaces between different dielectric phases (A and b), there will be a significant effect on the significance of the dielectric properties of the heterogenous material. Interfaces can create an apparent shift of the frequency position of molecular relaxation processes and broadening effects in their dielectric spectra. The internal interface is oriented with respect to the direction of the electric field applied.[8]

The inhomogeneity in various phases inside the dielectric material and at the sample-electrode interface results in space charge polarization. When frequencies are low, the charges are accumulated at the interface regions leading to the formation of interface polarizability. At low frequencies presence of different type of polarization results in high value of dielectric constant in all dielectric ceramics.[9] The electrons, ions, and other defects trap at these sites, which

have a slow response toward AC electric field. The response time varies from case to case, that is, 10^7 –10^-6 s.[10]

1.8 Arrhenius equation

Arrhenius equation was published in 1889. It gives very accurate depiction of the temperature dependence of the kinetics of simple chemical reactions. Based on the Arrhenius equation , at very low temperatures, reaction rates are very low but not zero. The Arrhenius equation has been widely used to obtain activation energies of charge carriers and dielectric relaxation processes in different ceramic materials to understand their conduction mechanism.

$$\tau = \tau_0 \exp\left(\frac{E_a}{kT}\right) \quad (8)$$

Where τ is relaxation period τ_0 is Pre-exponential Factor E_a activation energy k Boltzmann constant T absolute temperature. According to this equation, dipole relaxation is a thermally stimulated process in which big dipoles are frozen at low temperature. When τ drops at high temperatures exponential dipoles react quickly .[11]

1.9 Improvement needed in this field

As a new type of material, HEOCs had a relatively short research and development time and a complex and diverse composition system. At present, there is still a lack of theoretical support, and they are still gradually improved. Thus, the research on HEOCs in the future should focus on developing theoretical criteria for the design of HEOCs.[12]

2 Experimental Setup

Samples were prepared in University of Duisburg-Essen. Dielectric spectroscopy measurements were performed to investigate the dielectric properties of $(Ba_{0.2}Sr_{0.2}Ca_{0.2}La_{0.2}X_{0.2})TiO_3$ .In frequency range of 1.21 kHz to 1 MHz and temperature ranging from 10 K to 600 K for solid state rout prepared samples and 10 K to 300 K for sol-gel route prepared samples .The measurements were carried out using an HP4284A Precision LCR meter which allows accurate determination of capacitance and dielectric loss over a broad frequency range.

For dielectric measurement the samples were mounted in specially designed sample holders suitable for both heating and cooling measurements. The deposited metallic electrode on the ceramic surface gives reliable dielectric characteristics. The Keithley 2700 multimeter was connected to the sample holder and used to control the sample holder temperature during dielectric spectroscopy measurements.

A DC power supply was used to provide biasing and stable power to the instruments in measurement setup. The LCR meter Keithley 2700 multimeter and sample holder were electrically interconnected using appropriate connecting cables. During high temperature dielectric measurements, a coolant was employed to cool the sample holder. All instruments were interfaced with computer system for data acquisition. Measurement data was collected using new bridge and FVL power software which recorded the temperature dependent parameters. The acquired data was analysed using Origin software for data processing, graph plotting and to obtain the dielectric properties of the ceramics.

The area and thickness of the solid-state samples were as follows: $(Ba_{0.2}Sr_{0.2}Ca_{0.2}La_{0.2}Cs_{0.2})$area 53.739 and thickness 1.85mm $(Ba_{0.2}Sr_{0.2}Ca_{0.2}La_{0.2}K_{0.2})$area was 39.35 and thickness was 2.32mm $(Ba_{0.2}Sr_{0.2}Ca_{0.2}La_{0.2}Ag_{0.2})$area was 61.48 and thickness was 2.29mm $(Ba_{0.2}Sr_{0.2}Ca_{0.2}La_{0.2}Na_{0.2})$ area 56.63 and thickness was 1.59mm $(Ba_{0.2}Sr_{0.2}Ca_{0.2}La_{0.2}Li_{0.2})$area was 24.422 and thickness 2.29mm.The electrode was applied to both the surfaces of the ceramics and let it to dry for 30 to 40 minutes on each side. Then kept it for cooling in oven for heating at 500°C .The area and the thickness of the sol-gel samples were as follows : $(Ba_{0.2}Sr_{0.2}Ca_{0.2}La_{0.2}Cs_{0.2})$area 48.17 and thickness 1.31mm $(Ba_{0.2}Sr_{0.2}Ca0.2La_{0.2}K_{0.2})$area was 52.5 and thickness was 0.53 mm $(Ba_{0.2}Sr_{0.2}Ca_{0.2}La_{0.2}Ag_{0.2})$area was 21.94 and thickness was 0.36mm $(Ba_{0.2}Sr_{0.2}Ca_{0.2}La_{0.2}Na_{0.2})$ area 51.42 and thickness was 1.19mm $(Ba_{0.2}Sr_{0.2}Ca_{0.2}La_{0.2}Li_{0.2})$area was 55 and thickness 2.25mm. The electrode was applied to both the surfaces of

the ceramics and let it to dry for 30 to 40 minutes on each side. Then kept it for cooling in oven for heating at 500°C. For coaxial high frequency measurements, the specimens were prepared by cutting the solid-state samples into small pieces. The area and the thickness of them are as follows ($Ba_{0.2}Sr_{0.2}Ca_{0.2}La_{0.2}Cs_{0.2}$)area 4.538 and thickness 0.83mm ($Ba_{0.2}Sr_{0.}2Ca_{0.2}La_{0.2}K_{0.2}$) area was 4.35 and thickness was 0.87mm ($Ba_{0.2}Sr_{0.}2Ca0.2La\ _{0.2}Ag_{0.2}$) area was 4.077 and thickness was 0.55mm ($Ba_{0.2}Sr_{0.2}Ca_{0.2}La_{0.2}Na_{0.2}$) area 3.614 and thickness was 0.93mm ($Ba_{0.2}Sr_{0.}2Ca_{0.2}La\ _{0.2}Li_{0.2}$) area was 4.65 and thickness 1.06mm.

2.1 LCR meter

An electronic device called an LCR meter is used to measure characteristics like inductance (L), capacitance (C) and resistance (R) of an electronic component. The primary parameters that can be measured by the LCR meter are inductance (L), capacitance (C), resistance (R), magnitude of complex impedance (Z), magnitude of complex admittance (Y) and the conductance (G). The secondary parameters measured by the LCR meter are dielectric loss factor (D), quality factor (Q), phase angle (θ) etc. By putting the sample holder inside a furnace, the variation of these characteristics with the frequency of the applied electric field is examined both at room temperature and at high temperatures . Using related formulas, the capacitance C and loss tangent values received directly from the LCR meter readings can be used to determine the complex dielectric functions permittivity (ε^*) impedance (Z^*) ,modulus (M^*) and the AC conductivity of the dielectric material.

Dielectric parameters: The complex permittivity is given as:

$$\varepsilon^*(\omega)=\varepsilon'(\omega)-j\varepsilon''(\omega) \tag{5}$$

[ε' : real part, ε'' : imaginary part]

$$\varepsilon'(\omega)=\varepsilon_0 \frac{C_d}{\varepsilon_0 A} \tag{6}$$

d: the thickness of pellet, A: surface area of pellet ε_0: absolute permittivity/permittivity of free space

Dissipation factor:

$$\tan\delta = \frac{\varepsilon''}{\varepsilon'} = \frac{1}{\omega RC} = \frac{\sigma_{AC}}{\omega\varepsilon'} \tag{7}$$

R is the resistance C is the capacitance of the material [$\omega = 2\pi f$, frequency] .[13]

2.2 Use of Network Analyser and Coaxial Probe to determine Complex Permittivity

A vector network analyser system coupled with a coaxial probe is used to measure the permittivity of a material over several decades of microwave frequency as a stimulus response system. The measurement is represented in a very simple block diagram in figure 4. A vector network analyser is made up of a frequency source, signal separation devices and detectors. The stimulus for the incident signal is the frequency source. Since the incident and reflected waves travel along the same coaxial structure the signal separation devices are required to separate the incident wave and the reflected wave prior to detection. The detectors sense the magnitude and phase of the incident and reflected wave. The vector network analyser is used to measure the reflection coefficient (r_a) at the open end of the coax probe r is a complex number which is the ratio of the reflected wave to the reflected to the incident wave. The magnitude and phase of the reflection coefficient is dependent on the material characteristics of the sample in contact with the open end of the coax probe. [21]

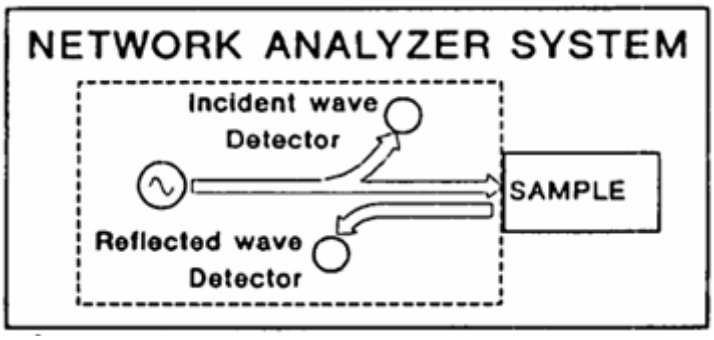

Figure 4. A block diagram of Network analyzer system.[21]

3 Results and Discussion of Solid-State Route Prepared Samples

3.1 Dielectric behaviour of $(Ba_{0.2}Sr_{0.2}Ca_{0.2}La_{0.2}Ag_{0.2})TiO_3$

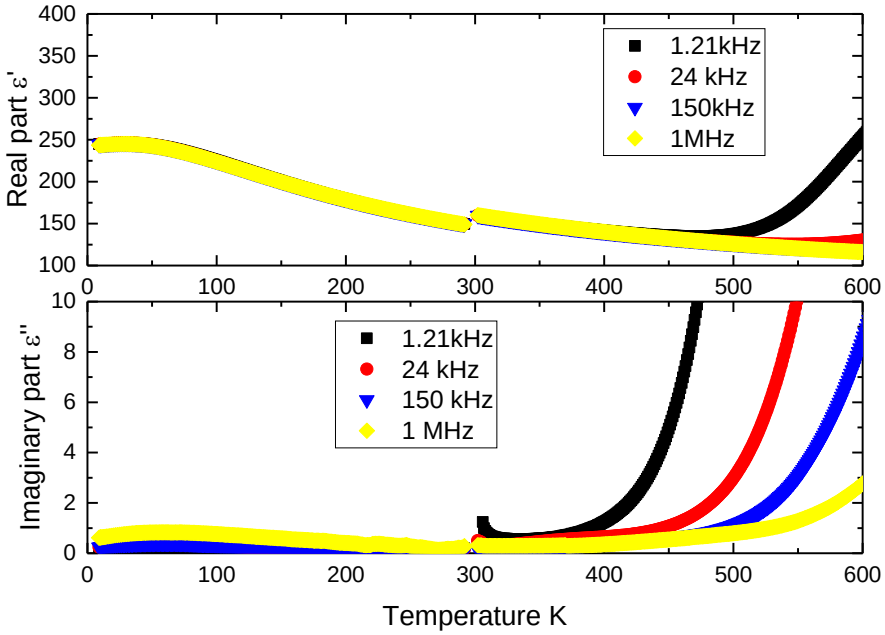

Figure 5. Temperature Dependence of Real and Imaginary parts of Dielectric permittivity of $(Ba_{0.2}Sr_{0.2}Ca_{0.2}La_{0.2}Ag_{0.2})TiO_3$ (HEC).

Figure 5 shows the Real and Imaginary part of dielectric permittivity versus Temperature. In Real part versus temperature, we see that in room temperature i.e. (300-350K) ε'decreases with increasing temperature for frequencies. In very low temperature dipoles are less mobile and cannot respond effectively to the applied field. The lowest frequency (1.21kHz) exhibits the highest real part of the ε'. At low frequencies, dipoles have sufficient time to respond to the applied electric field, resulting in enhanced dipolar alignment and a higher dielectric constant. This behaviour gives enhanced dielectric response. At lower frequencies a stronger dielectric response is observed because of slow polarisation mechanisms such as dipolar polarisation can follow the applied electric field. The effect is more pronounced at low frequencies because charge carriers have sufficient time to follow the applied electric field leading to polarisation and as temperature increases conductivity increases. In Imaginary part (ε'') the dielectric loss remains low at low temperatures showing minimal energy dissipation. As the temperature increases the imaginary part of the permittivity also increases and it is observed around 400K

at 1.21 kHz an increase in ε″ is noticeable. As temperature increases the mobility of charge carriers increases resulting in higher conductive losses . The dielectric loss is larger at low frequencies because charge carriers have sufficient time to follow the applied field, whereas at higher frequencies their response become limited.

3.2 Dielectric behaviour of $(Ba_{0.2}Sr_{0.2}Ca_{0.2}La_{0.2}Li_{0.2})TiO_3$

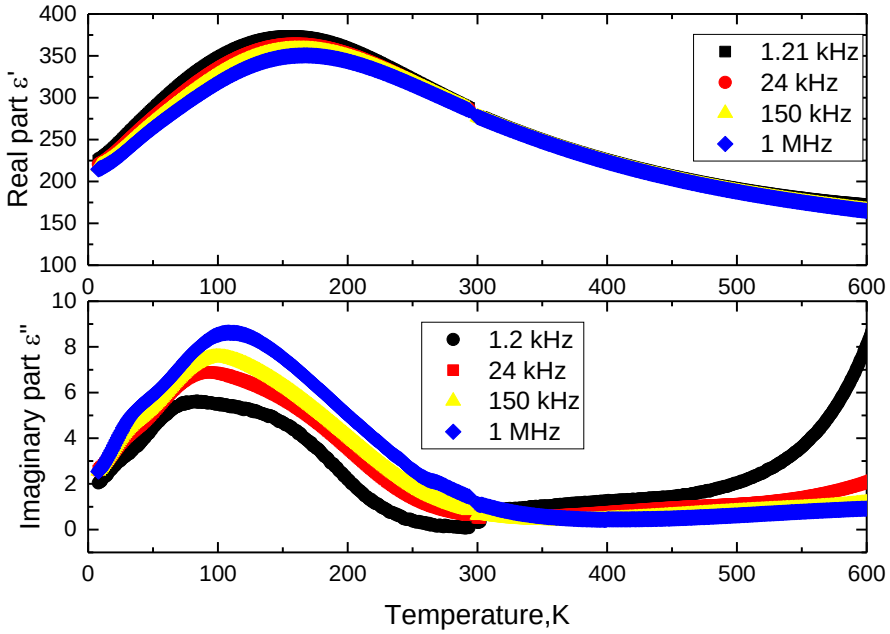

Figure 6. Temperature Dependence of Real and Imaginary parts of Dielectric permittivity $(Ba_{0.2}Sr_{0.2}Ca_{0.2}La_{0.2}\ Li_{0.2})TiO_3$ (HEC).

Figure 6 shows the Real and Imaginary part of dielectric permittivity versus Temperature. The real part ε' increases with temperature and reaches a maximum at (150-200K) for all measured frequencies then gradually decreases. Lower frequencies show high ε' values than higher frequencies saying that dipolar polarisation at lower frequencies can follow the applied field then higher frequencies. Here at temperature (150-200K) we see a peak because at this position thermally activated dielectric relaxation time of the dipole becomes comparable to the applied electric field. In this position dipolar reorientation is at most showing maximum polarization. At higher temperatures a tail like behaviour is observed at all frequencies this behaviour is attributed to increased conductivity due to thermally activated charge carriers which decreases

as temperature increases. The Imaginary part ε″ shows peaks at 100-200K.With increasing frequency the magnitude of ε″ decreases showing the Arrhenius behaviour .At low frequency (1.21 kHz) ε″ is indicating large dielectric losses. The peak represents the dielectric relaxation process. As the temperature increases dipoles gain enough energy to align with the external field. At high temperatures ε″ increases sharply at lower frequencies (1.21 kHz) while the increase is significantly supressed at higher frequencies (1 MHz) this behaviour is attributed to conduction losses. As temperature increases thermally activated charge carriers gain mobility leading to an increase in conductivity.

3.3 Dielectric behaviour of $(Ba_{0.2}Sr_{0.2}Ca_{0.2}La_{0.2}K_{0.2})TiO_3$

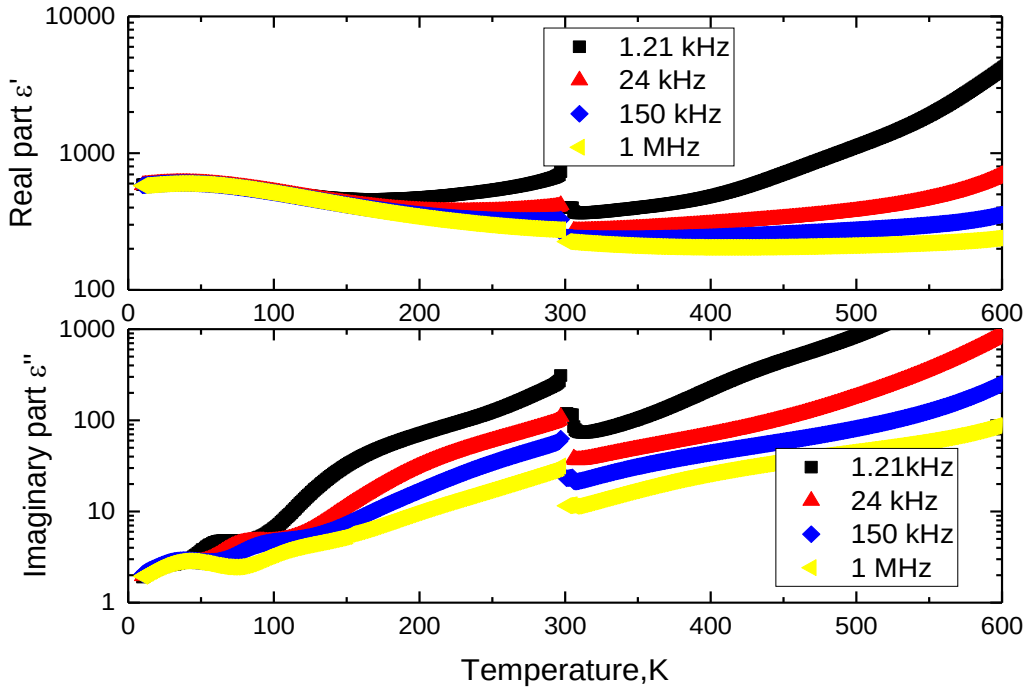

Figure 7. Temperature Dependence of Real and Imaginary parts of Dielectric permittivity $(Ba_{0.2}Sr_{0.2}Ca_{0.2}La_{0.2}\ K_{0.2})TiO_3$ (HEC)

Figure 7 shows the Real and Imaginary part of dielectric permittivity versus Temperature. In Real part ε'increases with temperature. At low temperature dipoles are not active as the temperature increases their movement starts. At lower frequencies ε' is higher because the dipoles have sufficient time to align with the applied field. On the other hand, at the higher frequencies the dipoles cannot follow the rapidly changing field resulting lower ε'. As the temperature increases dipoles become more mobile which enhances polarisation. At higher

temperature increased charge carrier mobility leads to enhanced conductivity . In Imaginary part we see smaller peaks at lower temperatures indicate dipole relaxation as the temperature increases dipoles gain enough energy to reorient with the field. A sharp increase in ε″ is observed this is attributed to Maxwell -Wagner interfacial polarization and the conductivity losses. The loss in the material becomes smaller when the frequency of the applied electric field increases.

3.4 Dielectric behaviour of $(Ba_{0.2}Sr_{0.2}Ca_{0.2}La_{0.2}Cs_{0.2})TiO_3$

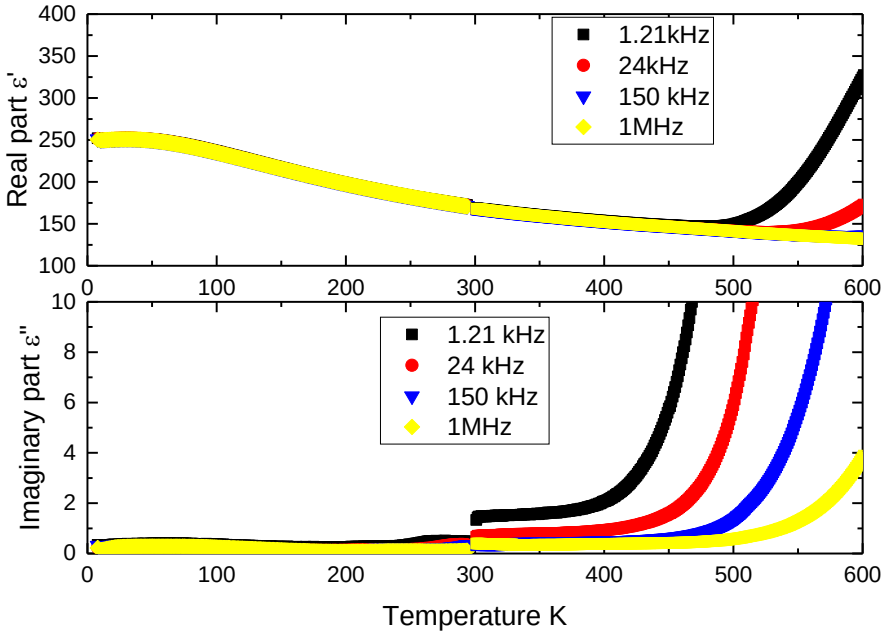

Figure 8. Temperature Dependence of Real and Imaginary parts of Dielectric permittivity $(Ba_{0.2}Sr_{0.2}Ca_{0.2}La_{0.2}\ Cs_{0.2})TiO_3$ (HEC).

Figure 8 shows the Real and Imaginary part of dielectric permittivity versus Temperature. In real part ε' decreases gradually with increasing temperature for all measured frequencies. This behaviour is attributed to the reduction of dipolar and space charge polarisation caused by thermal agitation. At high temperatures approximately 500K ε' decreases with increasing frequencies and it is related to the increased conductivity and thermally activated charge carriers. In imaginary part ε'' remains constant this indicates low dielectric loss. Beyond 500K dielectric loss increases sharply at low frequencies this behaviour is attributed to thermally activated conduction. This causes conduction losses at elevated temperatures. The dielectric

loss is highest at low frequency and decreases with increasing frequency because at low frequency fields allow charge carriers enough time to migrate so the losses are high whereas at high frequencies the carriers cannot follow the field.

3.5 Dielectric behaviour of $(Ba_{0.2}Sr_{0.2}Ca_{0.2}La_{0.2}Na_{0.2})TiO_3$

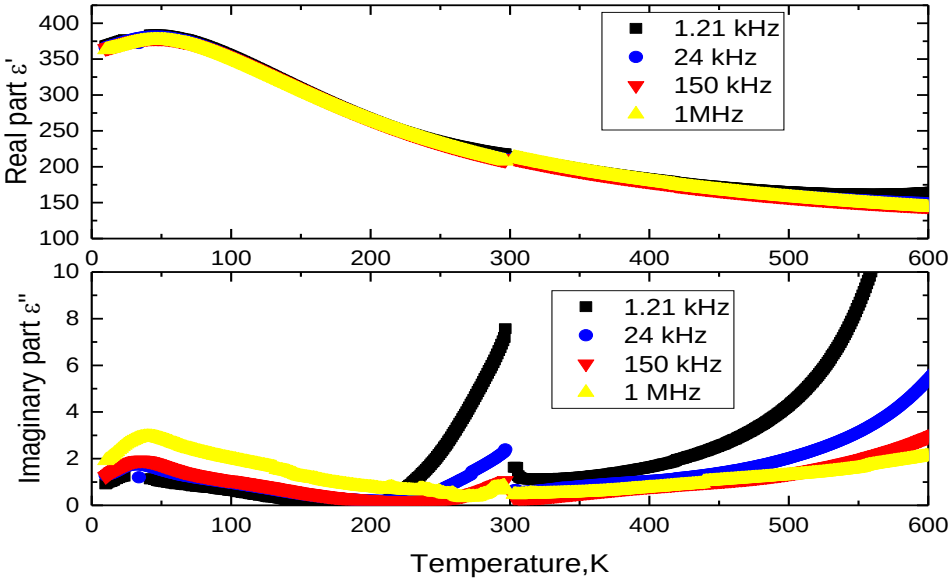

Figure 9. Temperature Dependence of Real and Imaginary parts of Dielectric permittivity $(Ba_{0.2}Sr_{0.2}Ca_{0.2}La_{0.2}Na_{0.2})TiO_3$ (HEC).

Figure 9 shows the Real and Imaginary part of dielectric permittivity versus Temperature. The real part ε' decreases with increasing temperature.As the temperature rises thermal agitation also increases which disturbs the alignment of dipoles. The value of ε' is higher at lower frequencies because the polarization mechanism has sufficient time to align with the applied field. Resulting in larger dielectric constant. At higher frequencies the applied field varies rapidly, and the dipoles are unable to reorient quickly to the field showing reduced polarization and lower ε'. At high temperatures ε' decreases because thermal agitation disrupts the alignment of charges and interfacial polarisation of charge carriers . In Imaginary part ε'' remains low at low temperatures due to the limited mobility of dipoles and charge carriers showing minimal loss. In higher temperature ε'' increases due to enhanced mobility of thermally activated carriers leading to conductivity loss. And this loss is high in lower frequency because they have time to follow the field. ε'' shows a higher response at lower

frequencies and lower frequencies at higher frequencies because at lower frequencies dipoles can effectively align with the applied field. As the frequency increases the dipoles and charge carriers are unable to follow the rapidly varying field, resulting in reduced energy dissipation.

3.6 Comparison graph

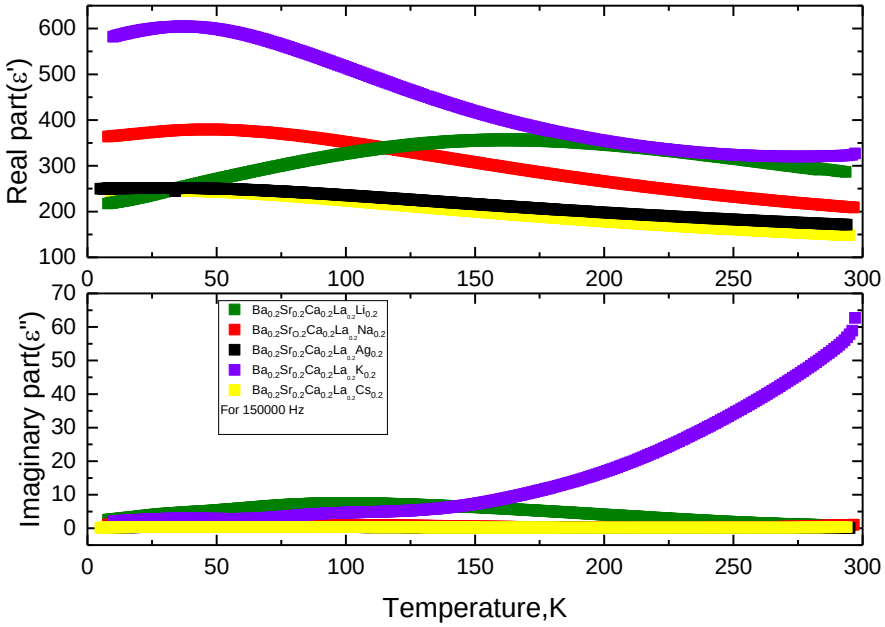

Figure 10. Temperature Dependence of Real and Imaginary parts of Dielectric permittivity at 150 kHz.

Table3 :Ionic radius of ions

Ion	Ionic Radius
Ag+	0.115nm [14]
Li^+	0.076nm [14]
Na^+	0.102nm [14]
K^+	0.138nm [14]
Cs^+	0.167nm [15]

The above graph shows the Temperature Dependence of Real and Imaginary parts of Dielectric permittivity at 150 kHz from 0K to 300K in real part at 150 kHz the dominant contribution is from space charge polarization. At low temperatures ions will occupy localized defect sites or interfaces leading to space charge accumulation. This charge accumulation enhances interfacial polarization resulting in high ε' values. At high temperatures with increasing in temperatures

ions gain sufficient thermal energy to escape trapping areas. The ability of ions to follow the electric field becomes limited and space charge polarization reduces. The high ε' is observed in ($Ba_{0.2}Sr_{0.}2Ca_{0.2}La_{0.2}K_{0.2}$) at low temperature due to ionic radius which causes stronger trapping of ions resulting enhanced space-charge polarization. In Imaginary part at low temperatures ions possess insufficient energy to move. As the result ε'' is low. As temperature increases thermal energy activates hopping between neighbouring sites the number of charge carriers increases the sharp rise is seen in ($Ba_{0.2}Sr_{0.2}Ca_{0.2}La_{0.2}K_{0.2}$) at high temperatures due to high mobility of K^+ ion indicating the conduction losses results in greater energy dissipation.

Table 4. Ions maximum temperature according to ionic radius

Ion	**Ionic Radius, nm**	**Ions Maximum temperature, K**
Ag^+	0.115 [14]	29
Li^+	0.076 [14]	163
Na^+	0.102 [14]	46
K^+	0.138 [14]	38
Cs^+	0.167 [15]	30

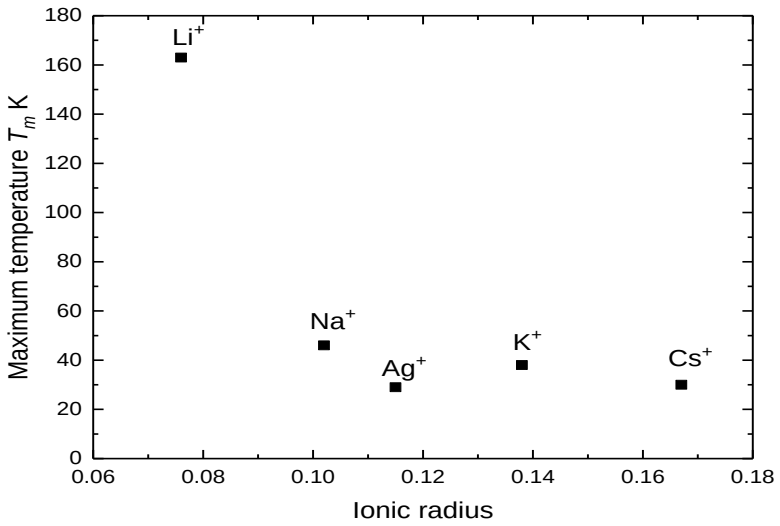

Figure 11. Ionic Radius dependent Maximum Dielectric Permittivity Temperature of Ions.

Figure 11 shows among the investigated ions K^+ demonstrates higher dielectric permittivity and dielectric loss despite of having lower T_m than other ions .This is behaviour is because of ionic radius and polarization of K^+ .With moderate ionic radius K^+ experiences weaker binding to the lattice compared to other ions, enabling easier displacement under an applied electric field. This enhanced ionic displacement contributes to ionic and space charge polarization, leading to increase in real and imaginary part. In contrast Li^+ ion despite exhibiting higher thermal stability show reduced dielectric response due to strong localization of Li^+ ions within the lattice, the smaller the ionic radius and strong interactions restrict ionic mobility thereby suppressing the polarization.

4 Results and Discussion of Sol Gel Route Prepared Samples

4.1 Temperature dependent Dielectric behaviour and comparison graph at 100K of sol-gel and solid state of ($Ba_{0.2}Sr_{0.2}Ca_{0.2}La_{0.2}Ag_{0.2}$) TiO_3

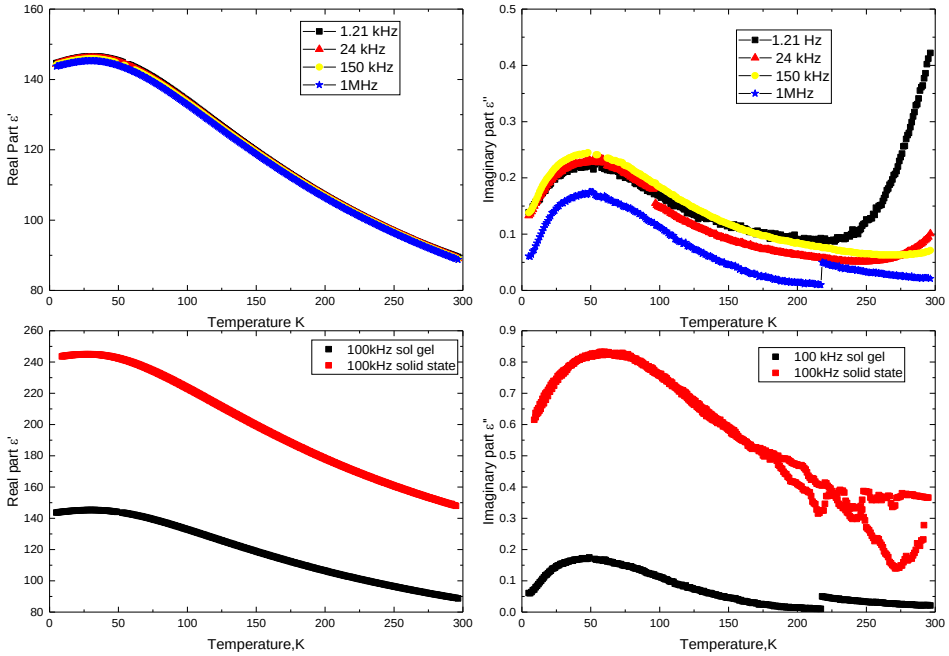

Figure 12. Temperature Dependence of Real and Imaginary parts of Dielectric permittivity of ($Ba_{0.2}Sr_{0.2}Ca_{0.2}La_{0.2}Ag_{0.2}$)$TiO_3$ (HEC) of sol gel .And comparison graph of sol-gel and solid-state real and imaginary part at 100 kHz.

Figure 12 shows the real and imaginary part of sol-gel material .Top left graph shows real part of permittivity that decreases gradual with increasing temperature from 0K to 300K for all measured frequencies . At low temperatures dipoles in the lattice are well aligned with the applied electric field in low temperature high polarisation and large ε′. As temperature increases thermal agitation of dipoles happens dipoles cannot follow the electric field as effectively .This causes a reduction in polarisation, leading to lower ε′. At higher frequencies 1MHz dipoles have less time to respond to the external field. Therefore ε′ becomes slightly lower compared with other low frequency measurements. In top right graph shows imaginary part of

permittivity which exhibits broad peak around 40-80K , followed by a decrease at higher temperature. Here the peak is due thermally activated dielectric relaxation time of the dipole becomes comparable to the applied electric field. In this position dipolar reorientation is at most showing maximum polarization. At low temperatures charge carriers remain immobile because they lack sufficient energy to move through the lattice. As temperature increases above 200K the thermal energy given to the system becomes large enough to activate the migration of the charge carriers . These charge carriers begin to hop between the lattices. This hopping causes energy dissipation which is shown the imaginary part this is especially visible at low frequencies (1.21 kHz) where the loss increases sharply above 230K. As the frequency increases dipoles cannot follow the field efficiently, so losses decrease. The bottom graphs show comparison between dielectric properties of the solid state and sol-gel samples at 100KHz. In the real part comparison, the solid-state samples show the higher ε' values compared to the sol-gel samples. This difference may arise from grain size effects that is solid state synthesis produces larger grains then sol-gel. Larger grains reduce grain boundary resistance . Sol-gel materials can contain more defects and smaller grain size and increased grain boundary resistance and more interfaces due to enhance Maxwell Wagner polarisation. In imaginary part comparison the solid-state samples exhibit significantly larger ε'' values indicating higher dielectric loss, while the sol-gel sample shows lower loss. Higher loss in solid-state is due to increased charge carrier mobility larger grains allow easier movement of charge carriers . Grain boundaries cause Maxwell-Wagner polarisation leading to higher losses. In contrast sol-gel produces finer grains increases grain-boundary resistance suppress charge carrier movement resulting reduced dielectric loss.

4.1.1 Frequency dependent Dielectric behaviour of $(Ba_{0.2}Sr_{0.2}Ca_{0.2}La_{0.2}Ag_{0.2})TiO_3$

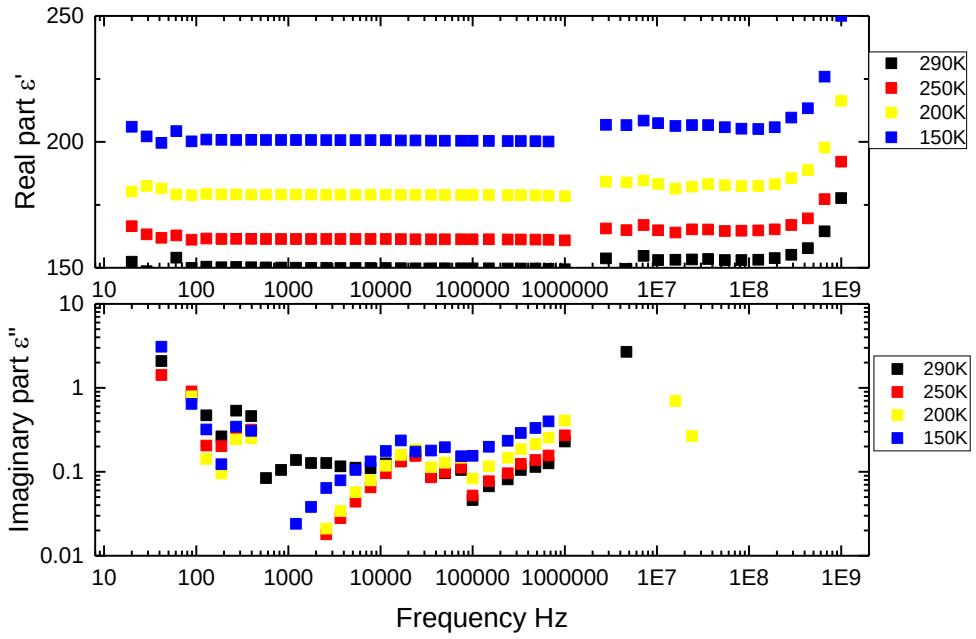

Figure 13. Frequency-dependent Real and Imaginary Dielectric permittivity of $(Ba_{0.2}Sr_{0.2}Ca_{0.2}La_{0.2}Ag_{0.2})TiO_3$ (HEC) of solid state.

The figure 13 shows the frequency dependence of the real and imaginary part of the $(Ba_{0.2}Sr_{0.2}Ca_{0.2}La_{0.2}Ag_{0.2})TiO_3$ (HEC) of solid state at different temperatures. The measurements are performed in low mid frequency measurement and high frequency coaxial measurement system. These two measurements together describe the complete dielectric response of the sample across a wide frequency spectrum. In the real part ε′ remains relatively constant at low and mid frequencies due to the combined effects of space charge, interfacial, dipolar polarization because the applied electric field changes slowly at low frequencies and charge carries have sufficient time to move and accumulate at the grain boundaries and interfaces . In the high frequencies (coaxial measurements) ε′ shows a slight increase due to electronic and ionic polarization mechanism as these polarization processes involve displacements of ions and electrons clouds within the crystal lattice. And charge carriers cannot follow the rapidly alternating electric field. In the imaginary part ε″ decreases with increasing frequency because at low frequency charge carrier migrate through the sample and accumulate at the grain boundaries which produces energy dissipation . At high frequency polarization mechanisms like interfacial polarisation cannot follow the electric field only electronic and

ionic polarization takes place. These are intrinsic mechanisms and are much faster and have low losses, so energy losses become less.

4.2 Temperature dependent Dielectric behaviour and comparison graph at 100K of sol-gel and solid state of ($Ba_{0.2}Sr_{0.2}Ca_{0.2}La_{0.2}Na_{0.2}$) TiO_3

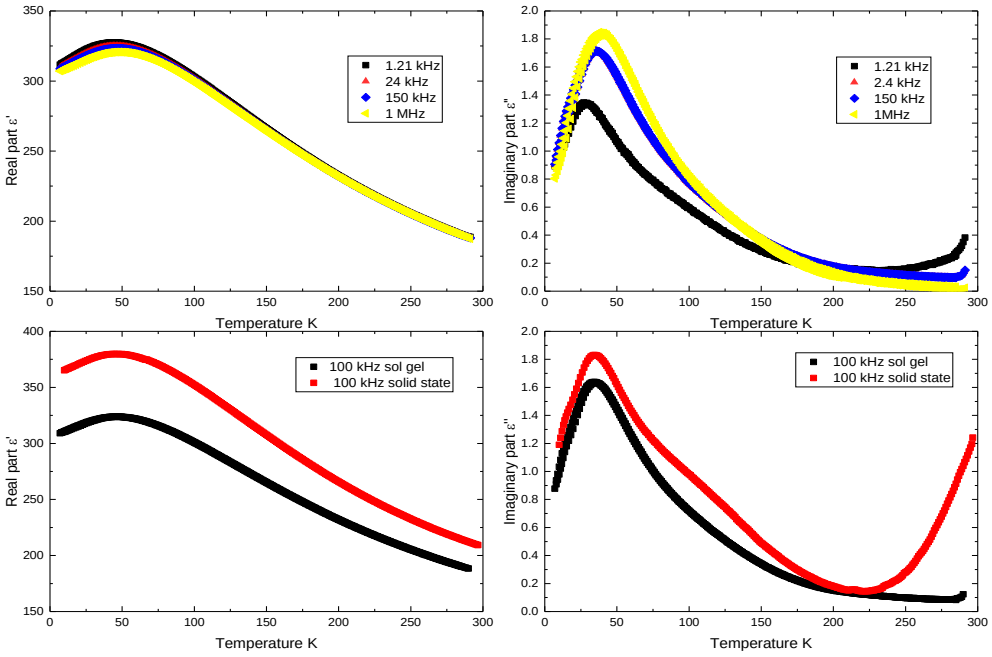

Figure 14. Temperature Dependence of Real and Imaginary parts of Dielectric permittivity of ($Ba_{0.2}Sr_{0.2}Ca_{0.2}La_{0.2}Na_{0.2}$)$TiO_3$ (HEC) of sol gel .And comparison graph of sol-gel and solid-state real and imaginary part at 100 kHz.

Figure 14 shows the real and imaginary part of sol-gel material .Top left graph shows real part of permittivity that decreases gradual with increasing temperature. At low temperatures dipoles are immobile. As temperature increases dipoles mobility increases allowing them to align more easily with the applied electric field. This causes the increases in dielectric constant .At the peak region around 40-70K the dipoles respond strongly to the electric field, producing a maximum in dielectric storage. At higher temperatures greater than 100K thermal agitation disturbs dipole alignment the polarization becomes less stable and the ε′ gradually decreases. At low frequencies dipoles have sufficient time to follow the electric field resulting higher ε′ as frequency increases dipoles cannot fully respond to the rapidly changing field so ε′

decreases. In imaginary part top right graph shows a peak around 40-60 K. At very low temperatures dipoles cannot follow the field effectively. As the temperature rises from around 40K the dipoles gain thermal energy and will begin to orient in response to the applied field and results in dissipation of energy as heat. When the dipoles become easier to orient the sample dissipates less energy and therefore ε'' decreases. The peak appears when the dipole relaxation becomes comparable to the applied field. At low frequencies charges have enough time to move which increases dielectric loss due to interfacial polarisation. This leads to increase in dielectric loss particularly at low frequencies where charge accumulation at grain boundaries occurs. Comparison graph between sol-gel and solid-state samples at 100 kHz the bottom let graph. In the bottom left graph, the sol-gel sample shows the lower ε' values while the solid-state sample exhibits significantly higher dielectric constant this is because the solid-state samples usually have larger grain size and lower grain boundary resistance. These effects increase the dielectric constant .On other hand sol-gel samples have smaller grains and has higher grain boundary resistance increased interfacial polarisation as a result ε' is lower. In imaginary part bottom right graph, we see a peak in 50 K in both the samples . The solid -state sample exhibits significantly higher dielectric loss the sol-gel sample shows lower loss across the temperature range. This is because solid-state samples show high loss due to enhanced charge carrier conduction increases energy dissipation. In contrast the sol-gel sample has higher grain boundary resistance and suppress the conduction losses results in lower dielectric loss.

4.2.1 Frequency dependent Dielectric behaviour of $(Ba_{0.2}Sr_{0.2}Ca_{0.2}La_{0.2}Na_{0.2})TiO_3$

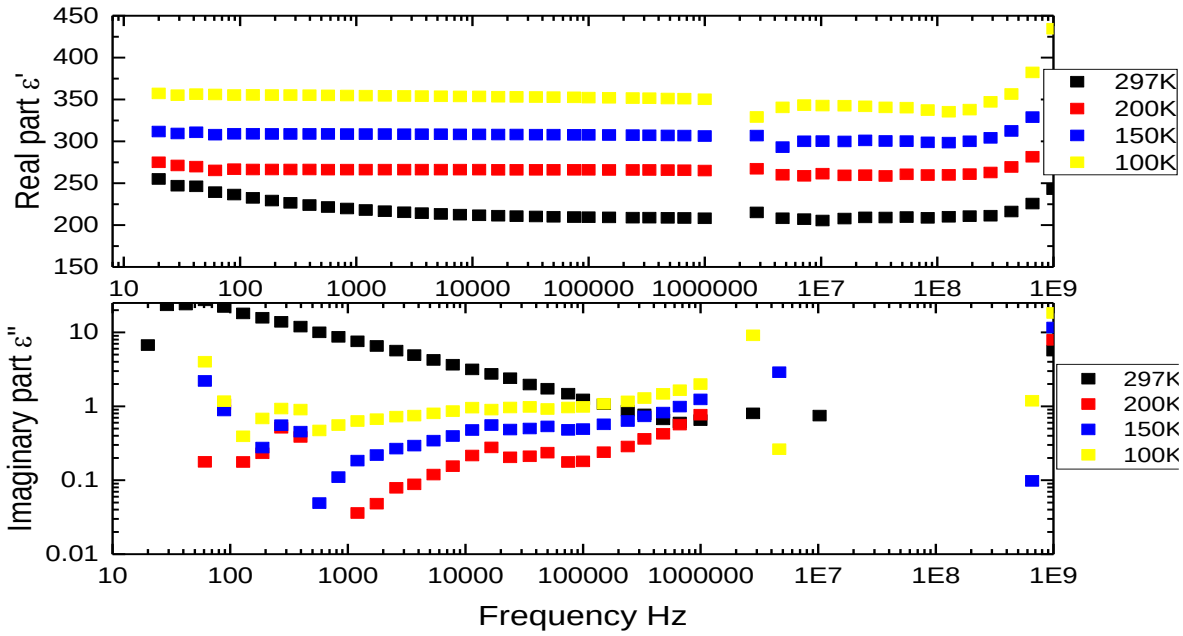

Figure 15. Frequency-dependent Real and Imaginary Dielectric permittivity of $(Ba_{0.2}Sr_{0.2}Ca_{0.2}La_{0.2}Na_{0.2})TiO_3$ (HEC) of solid state.

The figure 15 shows the frequency dependence of the real and imaginary part of the $(Ba_{0.2}Sr_{0.2}Ca_{0.2}La_{0.2}Na_{0.2})TiO_3$ (HEC) of solid state at different temperatures. The real part remains nearly constant over a wide frequency range. This indicates that the polarization mechanisms can respond effectively to the applied electric field . At lower frequencies slightly higher ε′ values arise from interfacial polarization where charge carriers accumulate at grain boundaries and interfaces .As the frequency increases, these slower polarization process cannot follow they rapidly changing electric field . Therefore, their effect decreases and the dielectric constant becomes more stable at higher frequencies where only faster polarization mechanisms such as ionic and electronic polarization are active. This indicates good dielectric stability of the material over a broad frequency range. The imaginary part which represents the energy dissipation shows at low frequencies the 297k curve shows comparatively high ε″ values due to enhanced space charge polarisation and thermally activated charge carriers. With increasing frequency ε″ interfacial polarisation cannot follow the electric field only electronic and ionic

polarization takes place. These are intrinsic mechanisms and are much faster and have low losses, so energy losses become less.

4.3 Temperature dependent Dielectric behaviour and comparison graph at 100K of sol-gel and solid state of ($Ba_{0.2}Sr_{0.2}Ca_{0.2}La_{0.2}K_{0.2}$) TiO_3

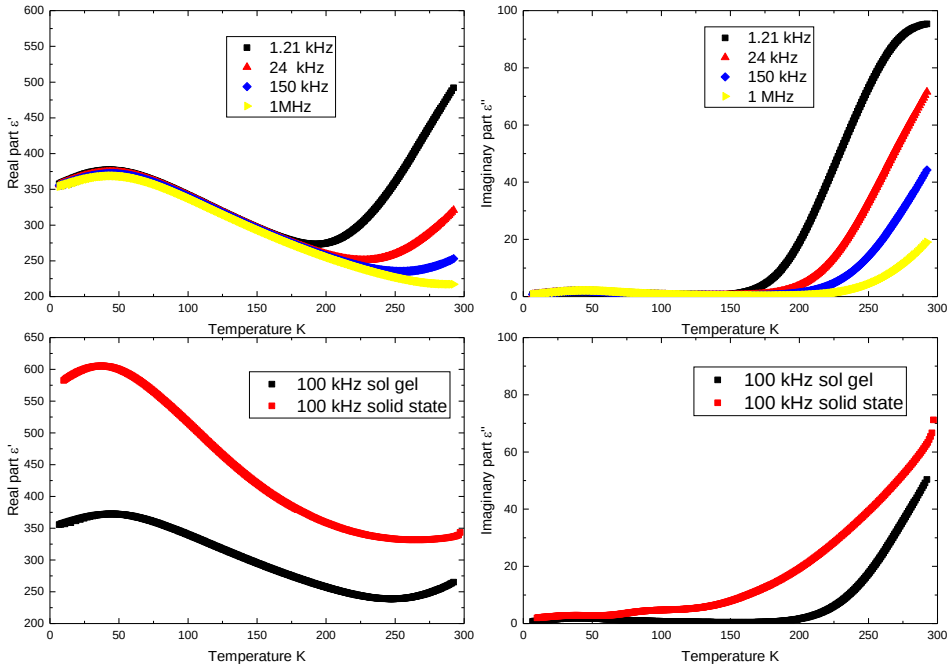

Figure 16. Temperature Dependence of Real and Imaginary parts of Dielectric permittivity of ($Ba_{0.2}Sr_{0.2}Ca_{0.2}La_{0.2}K_{0.2}$)$TiO_3$ (HEC) of sol gel .And comparison graph of sol-gel and solid-state real and imaginary part at 100 kHz.

Figure 16 shows the real and imaginary part of sol-gel material .Top left graph shows real part of permittivity is high due to dipolar polarization are strongly aligned with the electric field allowing material to store energy. As the temperature increases (50-200K) ε′ gradually decreases this is due to thermal agitation of dipoles reduced polarization alignment with the field . At higher temperatures (>200K) we have frequency dependent behaviour that is at low frequency 1.21kHz shows a sharp increase in ε′ and in higher frequencies show lower ε′ values. This is because of the interfacial polarization phenomenon and space charge accumulation at grain boundaries. At low frequencies dipoles and charge have sufficient time to follow the applied field , leading to higher polarization and larger dielectric constant. At higher frequencies the dipoles cannot respond quickly enough to the field resulting in lower ε′. At

imaginary part top right graph shows at low temperatures (<150K) ε″ remains small for all frequencies this shows minimal dipole mobility very low dielectric loss. As temperature increases beyond 170K ε″ rises significantly especially for low frequencies because of thermal energy activated dipoles polarization leading to energy dissipation. Charge carriers begin to migrate through the lattice and accumulate at interface contributing to energy loss. In frequency dependence lower frequencies exhibit higher ε″ values because dipoles and charge carriers can follow the electric field more easily. Whereas in higher frequencies charges carries and dipole cannot follow the field applied so losses decrease. Bottom left graph shows the comparison of sol-gel and solid state samples real part .Here the solid-state samples exhibit higher ε′ values across the entire temperature range this is due to larger grain size, reduced grain boundary density .In contrast sol -gel sample shows lower ε′ because they basically have smaller grains resulting in higher grain boundary density. In bottom right graph we have imaginary part of the comparison of sol-gel and solid -state sample here the solid-state sample has higher loss at higher temperatures this is due to increased charge carrier mobility and space charge accumulation on the other hand the sol-gel samples have lower ε″ values indicating reduced loss this is due to chemical homogeneity and increased grain boundaries resistance and suppress charge carrier mobility.

4.3.1 Frequency dependent Dielectric behaviour of $(Ba_{0.2}Sr_{0.2}Ca_{0.2}La_{0.2}K_{0.2})TiO_3$

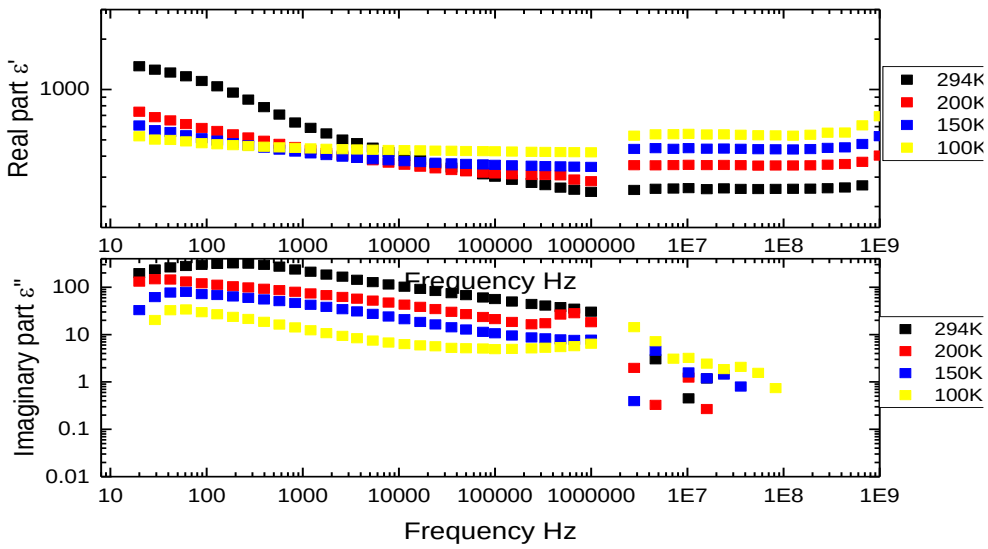

Figure 17. Frequency-dependent Real and Imaginary Dielectric permittivity of $(Ba_{0.2}Sr_{0.2}Ca_{0.2}La_{0.2}K_{0.2})TiO_3$ (HEC) of solid state.

The figure 17 shows the frequency dependence of the real and imaginary part of the $(Ba_{0.2}Sr_{0.2}Ca_{0.2}La_{0.2}K_{0.2})TiO_3$ (HEC) of solid state at different temperatures. In real part at low frequencies ε′ shows high values especially at 294K . This is mainly due to interfacial polarization and space charge polarization .Charge carriers accumulate at grain boundaries defects and in low frequencies charge carriers have sufficient time to align with the applied field this results in large polarisation and high dielectric constant the higher ε′ values in higher temperature occur due to increased thermal energy increases dipole mobility charge carriers can migrate more easily. In intermediate frequency region (10^3-10^6Hz) ε′ gradually decreases for all temperatures because of dipoles and space charges cannot respond fast enough to the rapidly oscillating field at higher frequencies (greater 10^7Hz) ε′ becomes nearly constant for each temperature . This indicates that intrinsic polarization mechanism mainly ionic and electronic polarizations have begun. These mechanisms occur extremely fast. In imaginary part at low frequencies ε″ values are very high especially at high temperatures this is due to space charge polarization at low frequencies charge carriers accumulate at grain boundaries defects and interfaces where they move under the applied field .This response causes significant energy dissipation resulting in large dielectric loss. The increase in ε″ with temperature indicates a thermally activated conduction process, where higher thermal energy enhances charge carrier mobility. In intermediate frequency region ε″ gradually decreases with increasing frequency this reduction occurs because charge carriers and dipoles are unable to follow the rapidly alternating field. As a result, space charge polarization and dipolar relaxation diminishes . At high frequency (greater than 10^7 Hz) ε″ becomes very small . At these frequencies slow polarization mechanisms such as space charge and dipolar polarization are suppressed since they cannot respond to the rapidly oscillating field . Therefore, only intrinsic polarization mechanisms mainly ionic and electronic polarization remain active . Resulting the samples exhibit very low dielectric loss in high frequency ranges.

4.4 Temperature dependent Dielectric behaviour and comparison graph at 100K of sol-gel and solid state of ($Ba_{0.2}Sr_{0.2}Ca_{0.2}La_{0.2}Cs_{0.2}$) TiO_3

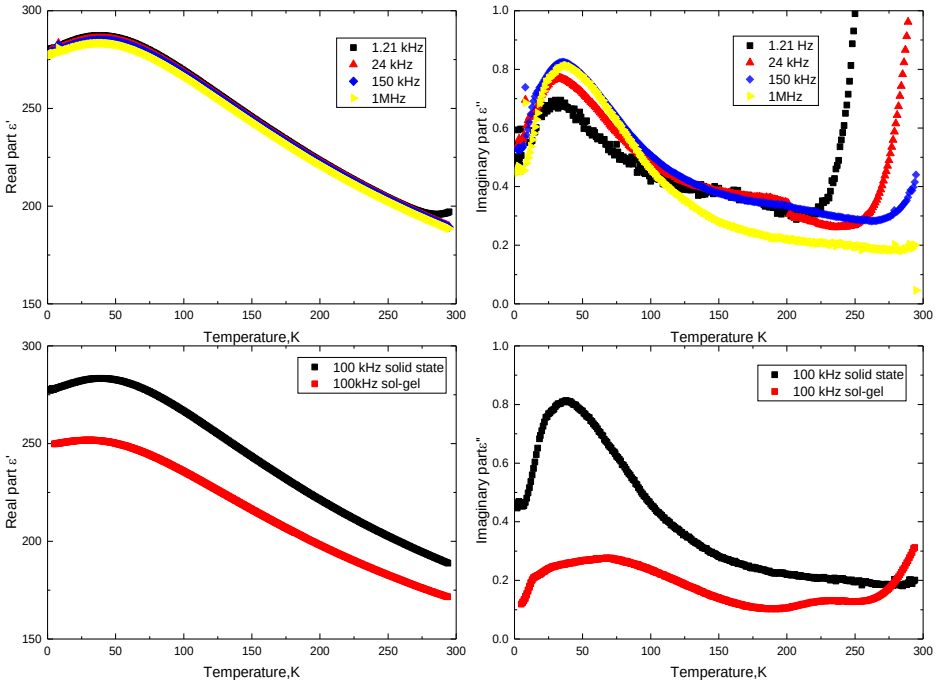

Figure 18. Temperature Dependence of Real and Imaginary parts of Dielectric permittivity of ($Ba_{0.2}Sr_{0.2}Ca_{0.2}La_{0.2}Cs_{0.2}$)$TiO_3$ (HEC) of sol gel .And comparison graph of sol-gel and solid-state real and imaginary part at 100 kHz.

Figure 18 shows the real and imaginary part of sol-gel material .Top left graph shows real part of permittivity that ε′ initially increases slightly with temperature around 40-60K . After the peak ε′ gradually decreases with increasing temperature this is because at low temperatures, dipoles have limited mobility as temperature (at peak) increases thermal activation increases dipole alignment polarization becomes stronger this leads to the initial increases in ε′. At higher temperatures ε′ decreases due to thermal agitation dipole alignment is disrupted due to this effective polarization decreases. In higher frequencies dipoles cannot follow the rapidly changing electric field . Thus ε′ decreases with increasing frequency. In imaginary part with increase in temperature a broad dielectric peak around 40-60K is seen which is due to enhanced dipolar polarisation. The highest dielectric constant is observed at low frequencies 1.21kHz because dipoles and charge carriers have sufficient time to align with electric field. As the

frequency increases the dielectric constant decreases due to the inability of dipoles to follow the rapidly changing electric field resulting in reduced polarisation. At higher temperature a significant rise especially in lower frequency region this is due to Maxwell Wagner polarisation. The bottom graphs show real and imaginary part of the sol-gel and solid-state synthesized samples at 100kHz .It is observed that at solid-state samples exhibit higher ε′ values indicating greater dielectric storage compared to the sol-gel sample due to the larger grain sizes. The imaginary part of the solid-state is higher which indicates increased dielectric loss. In contrast the sol-gel sample shows lower ε″ values indicating reduced energy dissipation. This behaviour is due to differences between grainsize charge carrier mobility and interfacial polarisation mechanisms.

4.4.1 Frequency dependent Dielectric behaviour of $(Ba_{0.2}Sr_{0.2}Ca_{0.2}La_{0.2}Cs_{0.2})TiO_3$

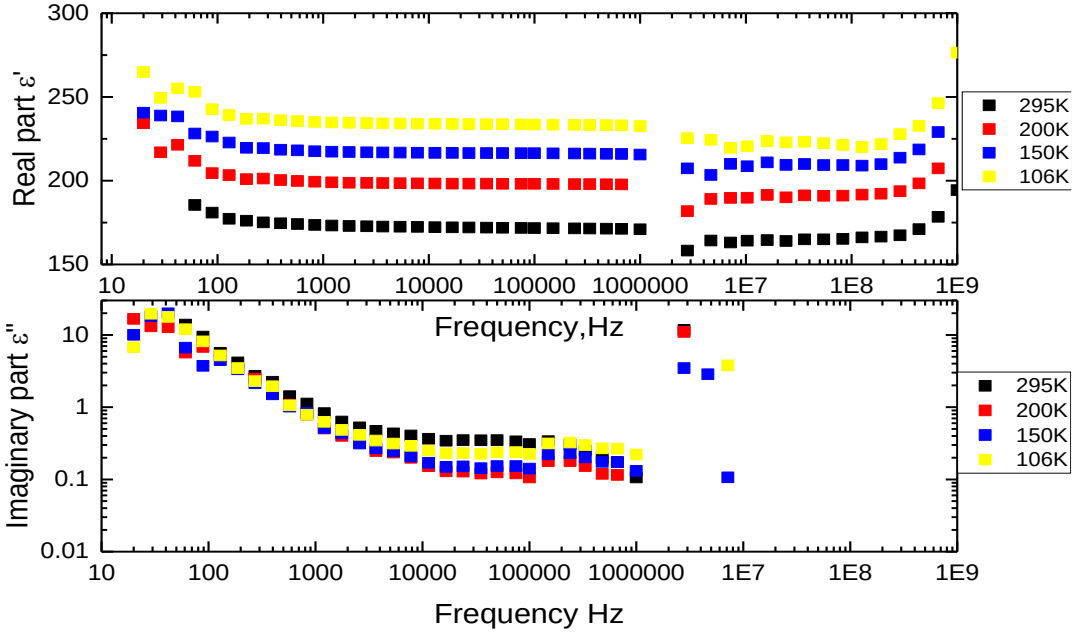

Figure 19. Frequency-dependent Real and Imaginary Dielectric permittivity of $(Ba_{0.2}Sr_{0.2}Ca_{0.2}La_{0.2}Cs_{0.2})TiO_3$ (HEC) of solid state.

The figure 19 shows the frequency dependence of the real and imaginary part of the $(Ba_{0.2}Sr_{0.2}Ca_{0.2}La_{0.2}K_{0.2})TiO_3$ (HEC) of solid-state at different temperatures. In real part at low frequencies ε′ shows relatively high values because of polarization mechanisms contribute to the dielectric response. As the frequency increases ε′ gradually decreases and tends to become nearly constant in the intermediate frequency region. This occurs because space charge and

dipole polarization cannot follow the rapidly alternating field at higher frequencies in the high frequency region above 10^7 Hz ε′ shows a slight increase in dispersion . This behaviour is associated with intrinsic polarization mechanism such as ionic and electronic polarization which respond to very high frequencies. Temperature also affects the permittivity values, where lower temperatures exhibit higher ε′ values while ε′ gradually decreases with increasing temperature due to reduced dipole alignment and increased thermal disorder. In imaginary part at low frequencies ε″ shows high values due to space charge polarization .As the frequency increases ε″ decreases rapidly because charge carriers cannot follow the electric field at higher frequencies which reduces energy dissipation in the high-frequency region ε″ becomes small. This indicates that dielectric loss is minimal at high frequencies showing good dielectric stability of the material over a wide range of frequency.

4.5 Temperature dependent Dielectric behaviour and comparison graph at 100K of sol-gel and solid state of ($Ba_{0.2}Sr_{0.2}Ca_{0.2}La_{0.2}Li_{0.2}$) TiO_3

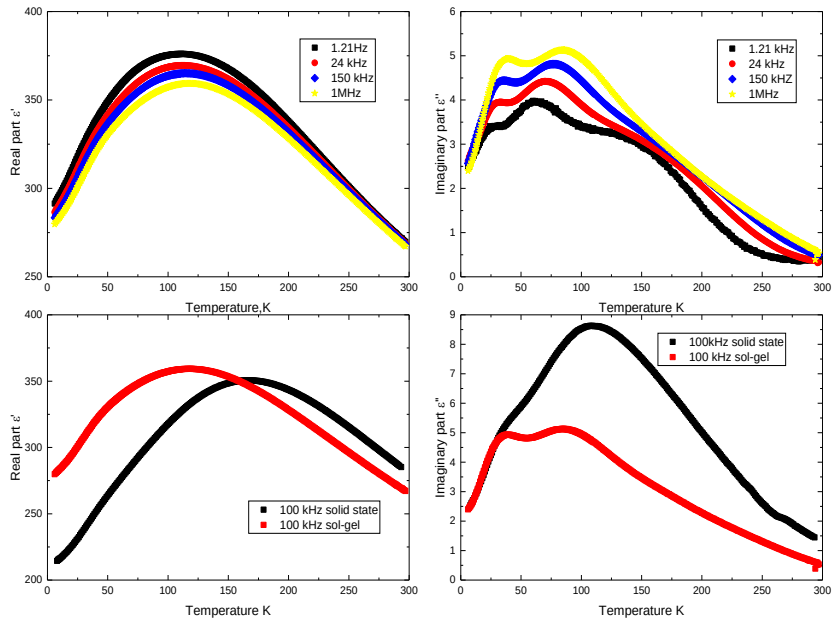

Figure 20. Temperature Dependence of Real and Imaginary parts of Dielectric permittivity of ($Ba_{0.2}Sr_{0.2}Ca_{0.2}La_{0.2}Li_{0.2}$)$TiO_3$ (HEC) of sol gel .And comparison graph of sol-gel and solid-state real and imaginary part at 100 kHz

Figure 20 shows the real and imaginary part of sol-gel material .Top left graph is the real part of permittivity that ε′ shows temperature and frequency dependence. At low temperatures the dipoles are frozen due to limited thermal energy. As the temperature increases thermal activation enhances dipole mobility under the applied electric field . This improves the polarization response of the sample resulting in an increase in storage density. In the intermediate temperature region, the material approaches a phase transition which is observed in perovskite systems. When the temperature increases further, thermal agitation begins to disrupt the dipole ordering within the lattice . The stability decreases and the polarization gradually weakens . As a result, storage density decreases at higher temperatures. At higher frequencies the dielectric fields change rapidly, and dipoles cannot fully align with the applied field. This dipole response reduces the polarization leading in reduction of storage density across different frequencies . In imaginary part energy loss increases with increasing temperature because the thermal activation enhances the mobility and dipole relaxation process. At moderate temperatures dipoles move more easily to the applied electric field and fluctuate more actively leading to increased energy dissipation. At higher temperatures increased conduction and interfacial polarisation leads to reduction in energy loss. At higher frequencies the electric field changes direction very quickly so the dipoles cannot follow it properly . The comparison graphs in bottom left and right shows real and imaginary part of sol-gel and solid-state samples. It is observed that the sol-gel synthesised sample exhibit higher energy storage density compared to the solid-state sample over the measured temperature range .This performance of sol-gel is mainly due to better chemical homogeneity and improved microstructure . In contrast the solid-state method produces larger grain and less uniform distribution these factors reduce the polarization efficiency of the material and reduces the energy storage density. The solid-state synthesised sample shows higher energy loss due to the presence of interfacial polarisation . These defects hinder efficient polarization which leads to greater energy dissipation. In contrast the sol-gel synthesised sample has better chemical homogeneity resulting in improved polarization behaviour and reduced loss.

4.3.1 Frequency dependent Dielectric behaviour $(Ba_{0.2}Sr_{0.2}Ca_{0.2}La_{0.2}Li_{0.2})TiO_3$

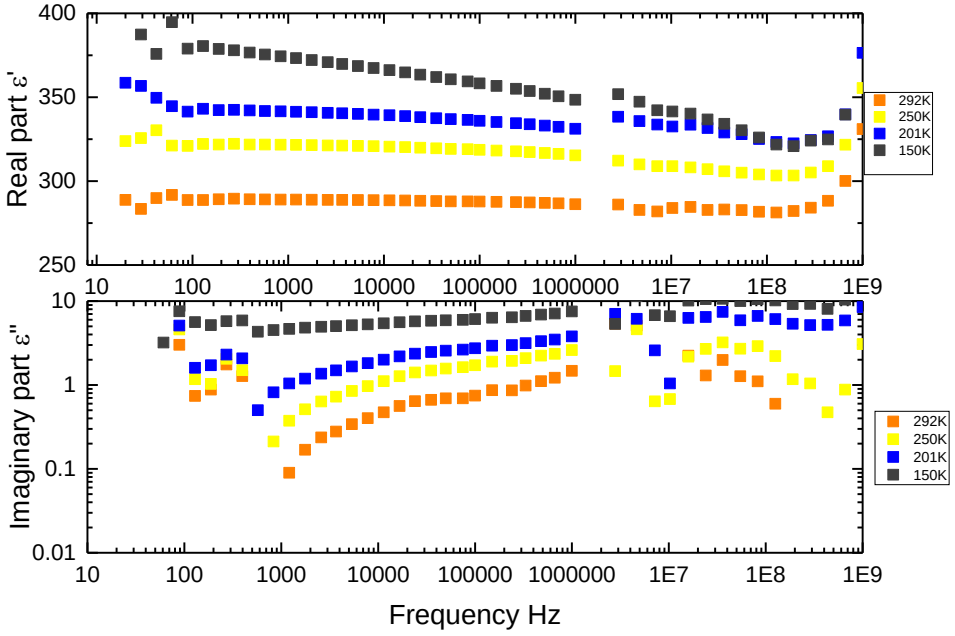

Figure 21. Frequency-dependent Real and Imaginary Dielectric permittivity of $(Ba_{0.2}Sr_{0.2}Ca_{0.2}La_{0.2}Li_{0.2})TiO_3$ (HEC) of solid state.

The above figure shows the frequency dependence of the real and imaginary part of the $(Ba_{0.2}Sr_{0.2}Ca_{0.2}La_{0.2}Li_{0.2})TiO_3$ (HEC) of solid-state at different temperatures. At low frequencies (10–10^3 Hz) ε′ is high at intermediate frequencies (10^3-10^6 Hz) ε′ gradually decreases with frequency at high frequencies ε′ drops. In low and intermediate frequency region ε′ is dominated by space-charge polarization at grain boundaries ,interfacial polarization charges have enough time to accumulate at interfaces results high ε′. This tells the larger ε′ at low frequencies. In intermediate frequency region as frequency increases dipoles and interfacial charges carriers cannot reorient quickly enough to follow the alternating field . In high frequency region (>10^7 Hz) only fast electronic and ionic polarizations can respond. In imaginary part at low frequency ε″ are slightly high at 150K. This occurs because charge carriers accumulate at grain boundaries and interface within the material. These accumulated chargers contribute to space charge polarization which causes higher dielectric loss due to energy dissipation . In the intermediate frequency the dipoles try to follow the applied electric field but cannot respond immediately. This response causes higher energy dissipation resulting in increased dielectric loss. At high frequencies (>10^7Hz) the dipoles and charge carriers

cannot respond to the rapidly changing electric field. Therefore, only fast electronic and ionic polarization remain active.

Conclusions

In the investigation of the dielectric properties of the studied samples over a wide temperature and frequency range of solid-state and sol-gel samples, it was determined that:

1. The shift in the dielectric permittivity maximum temperature is related to the different ionic radii of the substituents. The smaller the radius, the higher the temperature of dielectric permittivity maximum temperature.
2. $(Ba_{0.2}Sr_{0.2}Ca_{0.2}La_{0.2}Li_{0.2})TiO_3$,$(Ba_{0.2}Sr_{0.2}Ca_{0.2}La_{0.2}Na_{0.2})TiO_3$,$(Ba_{0.2}Sr_{0.2}Ca_{0.2}La_{0.2}K_{0.2})TiO_3$ samples exhibit two dielectric dispersions at low temperatures. They can clearly be observed from imaginary part of dielectric permittivity of solid-state route prepared samples.
3. Compared to the sol-gel route prepared sample, the solid-state route prepared sample exhibits a higher dielectric constant due to its larger grain size and higher dielectric loss caused by increased defect density, whereas the sol-gel route prepared sample shows a lower dielectric constant and lower dielectric loss because of its smaller grain size, higher grain boundary resistance, better chemical homogeneity and more refined microstructure.

References

[1] Wentao Yang Guangping Zheng High energy storage density and efficiency in nanostructured ($Bi_{0.2}$ $Na_{0.2}$ $K_{0.2}$ $La_{0.2}$ $Sr_{0.2}$)TiO_3 high entropy ceramics Journal of American Ceramic Society Volume 105 Pages 1083-1094 Year 2022.

[2] Jie wu, Jian Guo, Yifeng Ren,Yanping Yang,Ziyou Zhang,Hongliang Dong,Shan-Tao Zhang,Zhiqiang Chen, and Yu Deng High -Entropy la-($Bi_{0.2}$ $Na_{0.2}$ $Ba_{0.2}$ $Sr_{0.2}$ $Ca_{0,2}$)TiO3 Ceramic with ultrasonic Dielectric Performance within 327-689 K and up to7 Gpa.Advance electronic Materials Volume 10 Article ID 2400028 Pages 1-8 Year 2024.

[3] Sukhdeep Kaur,Manjit Sandhu,Jaipreet Kaur Dielectric Theory and its Properties International Journal of Emerging Technologies in Engineering (IJETER) Volume 4 Issue 3 Pages 145-150 Year 2016.

[4] Faouzia Tayari ,Silvia Soreto Teixeira,Manuel Pedro F.Graca and Kais Iben Nassar A Comprehensive Review of Recent Advances in perovskite materials:Electrical ,Dielectric and Magnetic Properties Inorganics Volume 13 Article number 67 Pages 2-34 Year 2025.

[5] Rajashree Khatua, S.K. Patri, S.K. Badjena Significant dielectric properties of high-entropy oxide ($Ba_{0.2}$ $Na_{0.2}$ $Ba_{0.2}$ $Sr_{0.2}$ $Ca_{0.2}$) TiO_3 Materials Today Communication Volume 42 Article ID 111343 Page 1-7 Year 2025.

[6] Gang Du Canhua Li Jiamao Li Guanghao Wu Zhenyi Hunag Aiqin Mao Mengchen Ma Zhiyun Guo Zhao Chen Research Progress on high entropy oxide ceramics:Principles,preparation and properties Journal of Materials Research and Technology Volume 35 Pages 265-288 Year 2025.

[7].Mokhtar Hjiri Anouar Jbeli Nouf Ahmed Althumairi N Mustapha Abdullah M Aldukhayel Ceramic perovskite via sol-gel processing: progress , challenges and applications Journal of Sol-Gel Science and Technology Volume 116 Pages 1630-1654 Year 2025.

[8] Mariem Samet,Ali Kallel,Anatoli Serghei Mawell-Wagner-Sillars interfacial polarisation in dielectric spectra of composite materials:Scaling laws and applications Journal of Composite Materials Volume 56 Issue 20 Pages 1-59 Year 2022.

[9] Haribabu Palneedi, Mahesh Peddigari, Geon-Tae Hwang, Dae-Yong Jeong,Jungho Ryu High-performance Dielectric Ceramic Films for Energy Storage Capacitors: Progress and Outlook Advanced Functional Materials Volume 28 Issue 42 Pages 1-33 Year 2018.

[10] Liu Hongbo Chapter 4 Dielectrics under Electric field Intech Open Journal Pages 74-89 Year 2018.

[11] Jan Khout Modified Arrhenius Equation in Materials Science, Chemistry and Biology National Library of Medicine Volume26 Article ID 7162 Pages 1-19 Year 2021.

[12] Sergey Shkuratav,Christopher S.Lynch A review of ferroelectric materials for high power devices Journal of Materials Volume 8 Page 739-752 Year 2022 .

[13] B.Biswal,D.K Mishra Review on LCR measurement of dielectrics and analysis of various parameters Orissa Journal of Physics Volume 31 Page 29-42 Year 2024.

[14] Masahiko Morinaga A Universal Relation Between Electron Density Minima and Atomic or Ionic Radii A Quantum Approach to Alloy Design Page 179-184 Year 2019.

[15] Julia Fernandez-Vidal Laurene J Hardick Gema Cabello Gary A Attard Effect of alkali-metal cation on oxygen adsorption at Pt single crystal electrodes in non-aqueous electrolytes Faraday Discussion Royal Society of Chemistry Volume 248 Page 102-118 Year 2024.

[16] Xi Kong, Letao Yang, Fangi Meng, Tao Zhang, Hejin Zhang, Yuan-Hua Lin, Houbing Huang, Shujun Zhang ,Jinming Guo,Ce-Wen Nan High-entropy engineered BaTiO3-based ceramic capacitors with greatly enhanced high-temperature energy storage performance Nature Communication Volume 16 Article number 885 Pages 1-9 Year 2025.

[17] Letao Yang,Xi Kong,Fei Li,Hua Hao,Zhenxiang Cheng,Hanxing Liu,Jing-Feng,Shujun Zhang Perovskite lead-free dielectrics for energy storage applications Progress in Material Science Volume 102 Pages72-108 Year 2019.

[18] Huimin Xiang, Yan Xing, Fu-Zhi Dai, Hongjie Wang, Lei Su, Lei Miao, Guojun Zhang, Yiguang Wang, X. Qi, Lei Yao, Hailong Wang, Biao Zhao, Jianqiang Li, Yanchun Zhou, High-Entropy ceramics: Present status, Challenges and a look forward Journal of Advanced Ceramics Volume 10 Pages 385-441Year 2021.

[19] SugatoHajra, Sushrisangtia Sahoo,Rutuparna Das,R.N.P. Choudhary Structural,Dielectric and Impedance Characteristics of $(Bi_{0.5}\ Na_{0.5})\ TiO_3$-$BaTiO_3$ electronic system Jornal of Alloys and Compounds Volume 750 Pages 507-514 Year 2018.

[20] Meenu Rani, Y.P Singh Shilpi Jindal Antiferroelectrics for Energy storage Applications: A Review International Journal of Creative Research Thoughts (IJCRT) Pages 42-47 Year 2022.

[21] David Blackham Use of Network Analyser and Coaxial Probe to Determine Complex Permittivity Hewlett-Packard Company Santa Rosa CA Volume 189 Pages 123-128 Year 1990.

[22] Faouzia Tayari, Kais Iben Nassar, Majdi Benamara, Manel Essid, Silvia Soreto Teixeira , M.P.F Graca Sol-Gel synthesised $(Bi_{0.5}Ba_{0.5}Ag)_{0.5}\ (NiMn)_{0.5}\ O_3$ perovskite ceramic :An exploration of its structural characteristics, dielectric properties and electrical conductivity Volume 50 Pages 11207-11215 Year 2024.

[23] Thomas Kleine-Ostmann Vector Network Analyser Chapter 4 THz Communications springer series in optical Sciences Volume 234 Page 29-36 Year 2022.

[24] J.de los Santos, D. Gracia, J.A. Eiras Dielectric Characterization of Materials at Microwave Frequency Range Materials Research Volume 6 Pages 97-101 Year 2002.

[25] A.Tkach, A. Almeida, J.Agostinho Moreria, J.Perez de la Cruz, Y.Romaguera-Barcelay Low-temperature dielectric response of $NaTaO_3$ ceramics and films Journal of America Institute of Physics Volume 100 Pages 1-5 Year 2012.

[26] Abdelhak El Ghandouri, Salaheddine Sayouri, Tajeddine Lamcharfi and Abdelhalim Elbasset Structural microstructure and dielectric properties of $Ba_{(1-x)}L_XTiO_{(1-x/4)}O_3$ prepared by sol gel method Journal of Advanced Dielectrics Volume 9 Pages 1-19 Year 2019.

[27] Roxana Elena Patru, Costantin Paul Ganea, Catalina-Andreea Stanciu, Vasile-Adrian Surdu, Roxana Trusca, Adelina-Carmen lanculescu, Ioana Pintilie, Lucian Pintilie (Ba,Sr) TiO_3 solid solution sintered from sol-gel derived powders:An insight into the composition and temperature dependent dielectric behaviour Journal of Ceramic International Volume 46 Pages 4180-4190 Year 2020.

[28] Eliezer M. Rabinovich Sol Gel Processing General Principles Journal of Sol-Gel Optics Pages 1-2 Year 1994.

[29] Junzhan Zhang, Shangyi Liu, Zhifeng Tian, Ying Zhang and Zongmo Shi The formation and Phase Stability of A-Site High-Entropy Perovskite Oxides Journal of Materials Volume 16 Pages 1-10 Year 2023.

[30] Wei Cai, Chunlin Fu, Jiacheng Gao, Xiaoyong Chen and Qiang Zhang Microstructure and Dielectric Properties of Barium Zirconate Titanate Ceramics by Two Methods Integrated Ferroelectrics: An International Journal of Integrated Ferroelectrics Volume 113 Pages 83-94 Year 2010.

[31] Georgios Giannoukos, Mart Min, Toomas Rang Relative complex permittivity and its dependence on Frequency World Journal of Engineering Relative complex permittivity and its dependence on Frequency Volume 14 Pages 532-537 Year 2017.

[32] Ashim Kumar and Prem Chand Pyroelectric Materials: Physics and Applications Chapter1 Fundamentals of Dielectrics Pages 1-17 Year 2023.

[33]. Sweety Supriya, Sunil Kumar and Manoranjan Kar Grain Size and Grain Boundary Effect on Dielectric Behaviour Of Nanocrystalline Cobalt Ferrite Nanotechnology Material and Devices Conference IEEE Pages 165-166 Year 2017.

[34]. Rezq Naji Aljawfi, F.Rahman, Khalid M. Batoo Effect of grain size and grain boundary defects on electrical and magnetic properties of Cr doped ZnO nanoparticles Journal of Molecular Structure Volume 1065-1066 Pages 199-204 Year 2014.

[35]. S.Ricote N.Bonanos, A.Manerbino, N.P.Sullivan W.G.Coors Effects of the fabrication process on the grain boundary resistance in $BaZr_{0.9}Y_{0.1}O_{3-\delta}$ Journal of Materials Chemistry A Volume 2 Pages 16107-16115 Year 2014.

Summary

This thesis focuses on the dielectric spectroscopy of high-entropy perovskite ceramics used for energy storage applications. The study investigates the dielectric properties of$(Ba_{0.2}Sr_{0.2}Ca_{0.2}La_{0.2}X_{0.2})TiO_3$ ceramics, where X represents Li, K, Na, Cs, and Ag. Both solid-state route and sol-gel route synthesis method were used to prepare the samples, and their dielectric behaviour was analysed over different temperatures and frequencies. The results show that dielectric properties depend strongly on temperature, frequency and ionic radius. Solid state samples generally exhibited higher dielectric constants but also higher dielectric losses due to their large grain size and defects while sol-gel samples exhibited lower dielectric loss this is due to their small grain sizes.

Šiame darbe tiriama didelės entropijos perovskitinių keramikų dielektrinės skvarbos dispersija. Tyrime tiriamos $(Ba_{0.2}Sr_{0.2}Ca_{0.2}La_{0.2}X_{0.2})TiO_3$ keramikų dielektrinės savybės, kur X reiškia Li, K, Na, Cs ir Ag. Mėginiai buvo paruošti tiek paprastos reakcijos metodu, tiek sol-gel metodu, o jų dielektrinės savybes buvo tiriamos skirtingose temperatūrose ir dažniuose. Rezultatai rodo, kad dielektrinės savybės stipriai priklauso nuo temperatūros, dažnio ir X jono joninio spindulio. Kietosios būsenos mėginiai paprastai pasižymėjo didesne dielektrine konstanta, bet taip pat didesniais dielektriniais nuostoliais dėl didelio grūdelių dydžio ir defektų, tuo tarpu sol-gel mėginiai pasižymėjo mažesniais dielektriniais nuostoliais dėl mažesnių grūdelių dydžių.